Tellus
SERIES B
CHEMICAL
AND PHYSICAL
METEOROLOGY
PUBLISHED BY THE INTERNATIONAL METEOROLOGICAL INSTITUTE IN STOCKHOLM

Tellus (2010), 62B, 441–454

TELLUS

Impact of entrainment from overshooting thermals on land–atmosphere interactions during summer 1999

By ERICA L. MCGRATH-SPANGLER* and A. SCOTT DENNING, *Department of Atmospheric Science, 1371 Campus Delivery, Colorado State University, Fort Collins, CO 80523-1371, USA*

(Manuscript received 19 November 2009; in final form 21 June 2010)

ABSTRACT

The depth of the planetary boundary layer (PBL) or mixed layer is important for carbon dioxide source/sink estimation because the response of atmospheric carbon dioxide concentration to a given amount of surface flux is inversely proportional to this depth. The PBL depth is affected by entrainment from overshooting thermals that is often underestimated in mesoscale meteorological models. An experiment was performed for the late summer of 1999 that includes a parameterization of PBL top entrainment that is based on a downward buoyancy flux at the top of the PBL. Simulations with this parameterization produce a warmer, drier and deeper boundary layer than a control simulation. The monthly mean diurnal cycle of PBL depth at a location in northern Wisconsin is better simulated with this enhanced entrainment when compared to observations. The altered atmospheric conditions cause the vegetation's stomata to respond and possibly close in an evolved response to limit water loss, thus reducing transpiration and shifting the Bowen ratio. The stomatal closing also reduces carbon assimilation, consequently altering horizontal and vertical carbon gradients. The overall effect of enhanced PBL entrainment is to alter time–mean regional gradients in CO_2 mixing ratio by as much as 7 ppmv over 1000 km.

1. Introduction

The response of carbon dioxide (CO_2) concentration to the surface fluxes of carbon is inversely proportional to the depth of the planetary boundary layer (PBL) (Denning et al., 1995; Yi et al., 2001, 2004). However, vertical turbulent mixing and PBL depth are not often simulated correctly by models (Denning et al., 1995, 1996a, 2008; Gurney et al., 2003) and an error in the depth of the PBL relates to an error in the modelled concentration of CO_2 in the boundary layer (Denning et al., 1995, 1996b, 1999, 2008; Zhang, 2002; Gerbig et al., 2003). CO_2 inversion studies are negatively impacted by an error in PBL depth because this translates to an error in the estimates of carbon sources and sinks (e.g. Gurney et al., 2002; Gerbig et al., 2003; Baker et al, 2006; Zupanski et al., 2007). For example, in a back of the envelope calculation, assuming a 10% increase in the PBL depth produces a 9% response in the CO_2 concentration. During the summer, this implies a higher daytime CO_2 concentration.

The PBL is a well-mixed layer in turbulent contact with the surface with weak vertical gradients and is capped by a temperature inversion. To resolve the PBL in models, high resolution is needed near the inversion, but a high concentration of model levels is excessive over the rest of the PBL. To complicate things further, because the depth of the PBL varies spatially and temporally, the height at which the added resolution is needed is also variable (Denning et al., 2008). The computational expense associated with including the number of model levels necessary to resolve the capping inversion for all of the different potential heights of the PBL is prohibitive.

PBL growth and development are controlled by small-scale processes that are generally not well resolved by mesoscale models (Ayotte et al., 1996; Gerbig et al., 2003). One such process is entrainment at the top of the boundary layer that is a result of rising thermals from the PBL overshooting their neutral level and pulling free tropospheric air into the PBL on their subsequent descent (Stull, 1988). Using the European Centre for Medium-Range Weather Forecasts (ECMWF) model, Beljaars and Betts (1992) found that the model produced conditions that were too cool and moist in a boundary layer that grew too slowly when simulating August conditions over the Konza prairie. After inclusion of an entrainment parameterization, their results improved indicating the importance of entrainment in numerical simulations. The PBL in the Regional Atmospheric Modelling System (RAMS) grows by encroachment as the surface warms, but does not include an explicit representation of PBL top entrainment, suggesting that important processes are not being represented. This process also alters the canopy air space (CAS) to which the

*Corresponding author.
e-mail: emcgrath@atmos.colostate.edu
DOI: 10.1111/j.1600-0889.2010.00482.x

vegetation responds by the incorporation of warmer and drier free tropospheric air into the mixed layer.

An entrainment parameterization (McGrath-Spangler et al., 2009) was introduced to the coupled ecosystem–atmosphere model SiB–RAMS (Denning et al., 2003; Nicholls et al., 2004; Wang et al., 2007; Corbin et al., 2008) based on the assumption that the downward buoyancy flux at the top of the PBL is proportional to the buoyancy flux at the surface (e.g. Betts, 1973; Carson, 1973; Deardorff, 1974; Rayment and Readings, 1974; Willis and Deardorff, 1974; Stull, 1976; Davis et al., 1997; Sullivan et al., 1998; Yi et al., 2001). It has been shown in idealized simulations that the introduction of this parameterization results in a warmer, drier and deeper PBL with a higher daytime concentration of CO_2 (McGrath-Spangler et al., 2009).

The primary objective of this study is to evaluate the performance of this parameterization in the summer of 1999 during which observations of PBL depth were being made at the WLEF very tall tower in northern Wisconsin (Angevine et al., 1998; Yi et al., 2001, 2004; Denning et al., 2008). The months of July, August and September of that year have observations at nearly an hourly timescale and provide a good timeframe for comparison. In addition, micrometeorological, eddy flux and CO_2 concentration measurements are made at several levels along the tower height providing a vertical profile (Yi et al., 2001, 2004; Davis et al., 2003; Denning et al., 2008). Other authors have examined the impact of subgrid-scale land surface heterogeneity on PBL processes, specifically the partitioning between sensible and latent heat fluxes due to variations in amount of vegetation cover (e.g. Avissar and Pielke, 1989; Pielke and Avissar, 1990; Avissar, 1991; Liu et al., 1999; Weaver and Avissar, 2001). This partition is important for determining PBL depth and induced mesoscale circulations. The emphasis of this paper, however, is not on mesoscale circulations, but on the local impact of overshooting thermals on entrainment and PBL growth. It would be interesting in the future to examine the impacts of both of these complex processes together.

Section 2 describes the SiB–RAMS model and the entrainment parameterization. Section 3 discusses the observations and measurement techniques. Section 4 illustrates the results and the final section provides some conclusions.

2. Methods

2.1. Model description

The ecosystem model in the coupled SiB–RAMS model is the third version of the Simple Biosphere (SiB3) model developed by Sellers et al. (1986). SiB3 calculates the transfer of energy, mass and momentum between the atmosphere and land surface (Sellers et al., 1996a, b; Corbin et al., 2008) and is coupled to the Brazilian version of the Regional Atmospheric Modelling System (BRAMS) (Freitas et al., 2006). Denning et al. (2003), Nicholls et al. (2004) and Wang et al. (2007) describe the coupled model in more detail.

The simulations presented here were performed on a single grid centred on the WLEF tower in northern Wisconsin. The grid used an increment of 40 km and spanned the continental United States and southern Canada. Vegetation data was derived from the 1-km AVHRR land cover classification data set (Hansen et al., 2000) while Normalized Difference Vegetation Index (NDVI) data were derived from 1-km resolution SPOT 10-day composites from the VEGETATION instrument on board the SPOT-4 (Système Probatoire d'Observation de la Terre) polar orbiting satellite. The NDVI data were provided by the United States Department of Agriculture Foreign Agriculture Service (USDA/FAS) through collaboration with the Global Inventory Modelling and Mapping Studies (GIMMS) Group at the National Aeronautics and Space Administration Goddard Space Flight Center (NASA/GSFC). Surface fluxes of carbon from anthropogenic sources are derived from 1995 CO_2 emission estimates from Andres et al. (1996) with a scale of 1.1055 to adjust for 1999 values (Marland et al., 2005; Wang et al., 2007). Air–sea CO_2 fluxes are the monthly 1995 estimates from Takahashi et al. (2002) and are assumed to adequately represent the conditions present in 1999.

Meteorological fields are initialized by the National Center for Environmental Prediction (NCEP) mesoscale Eta-212 grid reanalysis with 40-km horizontal resolution (AWIPS 40-k). This data set was also used to nudge the lateral boundary conditions every 30 min. Soil respiration factors and soil moisture were initialized from an offline SiB3 simulation run for 10 years using NCEP/NCAR (National Center for Atmospheric Research) reanalysis driver data from 1989 to 1999. Initial and hourly lateral boundary CO_2 concentrations were specified by the Parameterized Chemistry Transport Model (PCTM) (Kawa et al., 2004; Parazoo et al., 2008).

2.2. Entrainment parameterization

The entrainment parameterization was discussed in an idealized case study by McGrath-Spangler et al. (2009) and is based on the idea that the buoyancy flux at the top of the PBL is negatively proportional to the buoyancy flux at the surface (e.g. Betts, 1973; Carson, 1973; Deardorff, 1974; Rayment and Readings, 1974; Willis and Deardorff, 1974; Stull, 1976, 1988; Davis et al., 1997; Sullivan et al., 1998; Yi et al., 2001). The profile of buoyancy flux throughout the well-mixed, quasi-steady boundary layer is often approximated as linear, decreasing from the surface and becoming negative within the entrainment zone (Stull, 1976). This implies that the negative buoyancy flux at the base of the capping inversion is linearly proportional to the buoyancy flux at the surface. This assumption produces the equation:

$$\overline{w'\theta_v'}|_{Z_i} = -\alpha \overline{w'\theta_v'}|_s. \quad (1)$$

In eq. (1), $\overline{w'\theta'_v}$ is the turbulent virtual potential temperature flux at the height of the inversion (Z_i) and at the surface (s) and α is the tunable proportionality constant. Estimates of α range from zero to one, but most published values are between 0.1 and 0.3 with a value of 0.2 being the most appropriate for free convection (Stull, 1988).

Eq. (1) can be used to derive equations for the time rate of change of potential temperature, wind velocity, water vapour mixing ratio, turbulent kinetic energy (TKE) and CO_2 concentration across the interface separating the PBL from the overlying inversion. These equations mix the properties of the boundary layer with those of the free troposphere as would be done by overshooting thermals in the physical world. The result is warmer, drier, less turbulent conditions being mixed into the top model layer of the PBL to be mixed downward by turbulent eddies and cooler, moister, turbulent air being mixed up into the lowest layer of the overlying inversion.

In idealized simulations, the parameterization resulted in an insertion of heat energy into the PBL and an upward transport of TKE into the lowest layer of the overlying inversion, producing a deeper PBL. The downward advection of heat and upward moisture transport induced a warmer and drier boundary layer and a cooler and moister inversion layer.

The drying and warming caused by entrainment increases physiological stress thereby limiting carbon assimilation by plants. When conditions within the atmosphere in the immediate vicinity of the leaf become less than optimal, the stomata close, limiting water loss through transpiration and reducing carbon assimilation. This increases the Bowen ratio (the ratio of sensible to latent heat fluxes) as latent heat flux is reduced in favour of sensible heat flux. Increased sensible heat flux raises temperatures and encourages further PBL growth. In addition, changes to cloud cover and precipitation result from the shift in the Bowen ratio and multiple interrelated processes.

3. Observations

Evaluation of the entrainment parameterization uses observations from the WLEF television tower located in the Park Falls Ranger District of the Chequamegon National Forest, about 15 km east of Park Falls, Wisconsin, USA, at 45.95°N latitude, 90.27°W longitude.

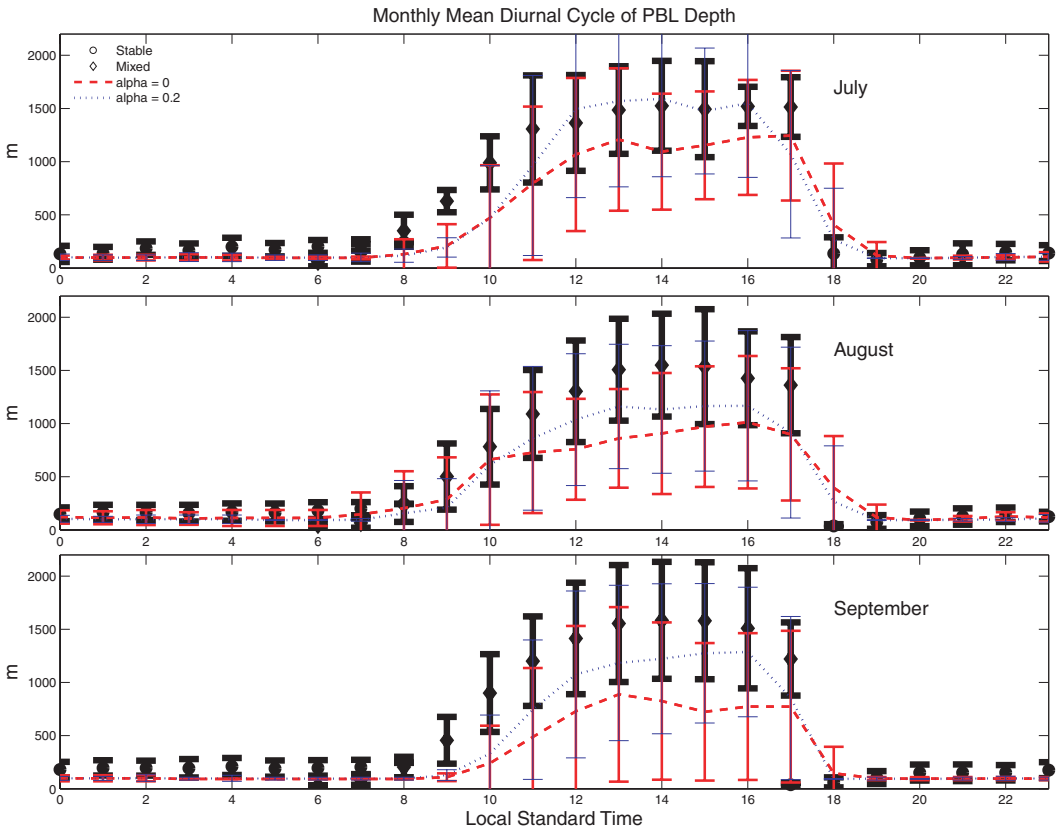

Fig. 1. Monthly mean diurnal cycle of PBL depth (m) in (a) July, (b) August and (c) September. Model estimates are averaged over non-precipitating hours only. Error bars are the standard deviation of daily values at each hour. The thickest error bars are for the observations, the next thickest are for the control case and the thinnest error bars are for the enhanced entrainment case.

Since 1996, micrometeorological and eddy covariance flux measurements have been made at 30 m, 122 m and 396 m (Berger et al., 2001; Davis et al., 2003). High precision, high accuracy CO_2 concentrations have been made at six levels (11 m, 30 m, 76 m, 122 m, 244 m and 396 m) since 1994. The CO_2 measurements are made using LI-COR 6251 infrared gas analysers (IRGA) (Bakwin et al., 1998; Davis et al. 2003).

During 1999, from July to September, an Integrated Sounding System (ISS) was deployed about 8 km east of the WLEF tower (Angevine et al., 1998; Yi et al., 2001, 2004; Denning et al., 2008). The ISS included a radar profiler, a Radar and Radio-Acoustic Sounding System (RASS), and a radiosonde (Yi et al., 2001). The profiler is a sensitive 915 MHz Doppler radar designed to respond to fluctuations of the refractive index in clear air (Ecklund et al., 1988; White et al., 1991; Angevine et al., 1993, 1994a, b; Yi et al., 2001) and can be used to detect the height of the PBL in conditions without precipitation or heavy clouds (Yi et al., 2001, 2004).

Boundary layers shallower than 400 m, such as those that occur at night and in the early morning, are not well defined from the profiler signal-to-noise ratio (SNR) measurements (Yi et al., 2001, 2004). In these cases, the strong stratification present in the nocturnal boundary layer produces a gradient in the CO_2 concentration (Yi et al., 2001, 2004; Denning et al., 2008) that is detected by the vertical profile of CO_2 measured along the depth of the tower and can be used to determine the depth of the nocturnal boundary layer.

4. Results

4.1. WLEF comparison

Figure 1 compares the observed monthly mean diurnal cycle of PBL depth measured near the WLEF tower in northern Wisconsin to the SiB–RAMS model for both the control ($\alpha = 0$) and enhanced entrainment cases ($\alpha = 0.2$). The error bars on the observations (thickest bars), control case (medium thickness) and enhanced entrainment case (thinnest bars) represent the standard deviation of daily values at each hour. Modelled daytime and nighttime PBL depths are determined by the potential temperature and CO_2 concentration gradients, respectively. The simulated monthly mean diurnal cycle was found by averaging non-precipitating hours to account for the lack of observations during precipitation events.

In all three months shown in Fig. 1, the enhanced entrainment case performed better in representing the observations than did

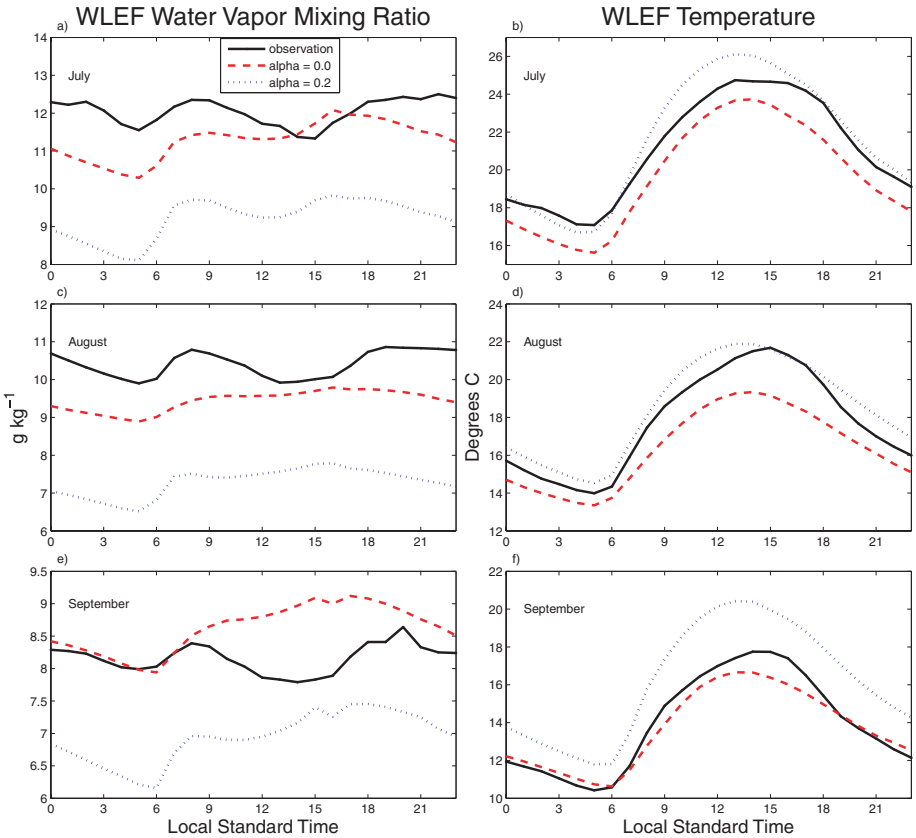

Fig. 2. Monthly mean diurnal cycle at WLEF of water vapour mixing ratio (g kg^{-1}) in the left column and temperature (°C) in the right column for July (a and b), August (c and d) and September (e and f) at 30 m.

the control case. Although the afternoon PBL depths in the control case fell within the error bars in July and August, these values were near the low end, especially in August, and were well below the observations and their associated error bars in September. This was partly due to the model's inadequate representation of the rapid late morning growth of the PBL that is better simulated in the enhanced entrainment case. Because nighttime values of PBL depth are similar for both model simulations, the steeper morning growth of the enhanced entrainment case produces a deeper PBL in the early afternoon that continues into the afternoon when PBL growth begins to slowdown. The enhanced entrainment simulation performed better in the afternoon as well with deeper maximum PBL depths in all three months, falling within the error bars. However, this simulation produced PBL depths that were still too shallow in August and September, indicating a need for further improvements.

PBL depth has large implications for CO_2 concentrations and gradients within the boundary layer. Deeper PBL depths dilute the effect of assimilation on carbon concentrations and the warming and drying associated with entrainment alters the stomatal openings of vegetation and therefore the uptake of CO_2. Accurately simulating CO_2 concentration is important for determining sources and sinks through atmospheric inversions and thus it is important to accurately simulate the PBL depth.

Figure 2 shows the differences in water vapour mixing ratio and temperature in July (a, b), August (c, d) and September (e, f) produced by the two model simulations compared to the observations. In general, the parameterization of overshooting thermals produced warmer and drier results, with mixed success. Water vapour was better simulated in the control simulations. Only in the mid-afternoon of September was the mixing ratio too moist and a drying improved the results. Although the mixing ratio was poorly simulated by the enhanced entrainment case in July and August, the warming associated with the enhanced entrainment improved the temperature in these months and even warmed a little too much in July. In September, the control simulation better represented the temperature.

Figure 3 presents the modifications of additional entrainment on net ecosystem exchange (NEE; respiration—carbon assimilation) (a, c, e) and CO_2 concentration (b, d, f) at 30 m at the WLEF tower during the summer of 1999. Too much uptake occurred in the morning and late afternoon of both cases, a known issue in SiB at the WLEF tower (Baker et al., 2003). The enhanced entrainment case was warmer in the early morning, allowing plant stomata to open earlier and begin carbon assimilation. The

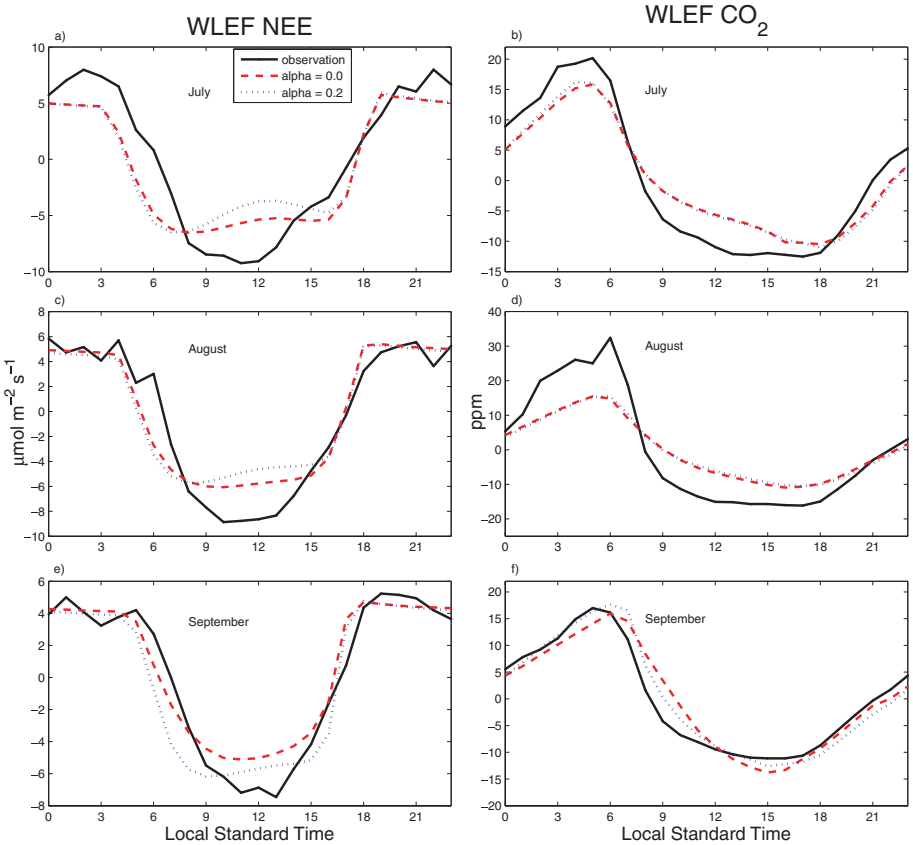

Fig. 3. Monthly mean diurnal cycles at WLEF of net ecosystem exchange (μmol m^{-2} s^{-1}) in the left column and of CO_2 concentration perturbations (ppmv) in the right column during July (a and b), August (c and d) and September (e and f) at 30 m.

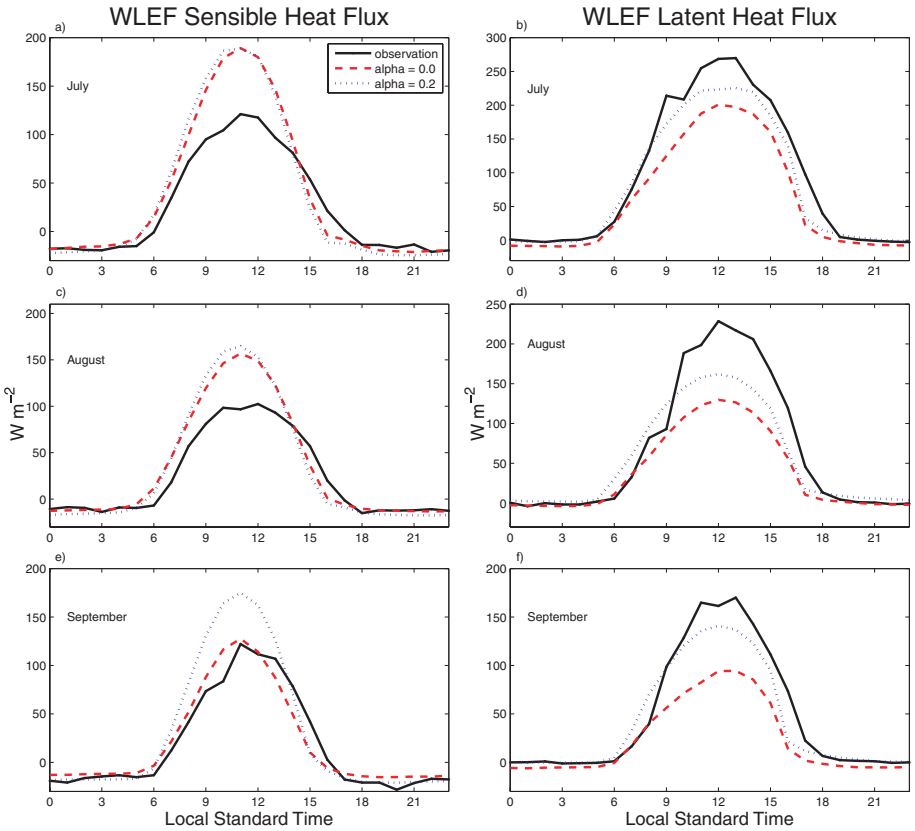

Fig. 4. Monthly mean diurnal cycle at WLEF of sensible heat flux (W m^{-2}) in the left column and of latent heat flux (W m^{-2}) in the right column during July (a and b), August (c and d) and September (e and f) at 30 m.

warmer and drier conditions at midday reduced stomatal conductance in the enhanced entrainment case, reducing carbon uptake to minimize water loss. In August, the control case produced a better estimate of NEE summed over the diurnal cycle, but in July and September, the additional entrainment produced better results.

The differences in CO_2 concentration at WLEF between the control and enhanced entrainment cases are small because of the conditions at WLEF during the simulation time frame. During these three months, northern Wisconsin is relatively unstressed and is not experiencing much water limitation. The warmer and drier conditions associated with enhanced PBL top entrainment do not change these overall conditions and the ecophysiological stress is only minimally changed so NEE (Fig. 10) is not much affected. However, even these small changes accumulate over time and, along with the changes in PBL depth, produce regional changes in CO_2 concentration (Fig. 11).

Figure 4 illustrates the differences in sensible (a, c, e) and latent (b, d, f) heat fluxes. The variations in the heat fluxes between the control and enhanced entrainment cases demonstrate the interactions between the PBL, the physiological responses and the large-scale weather. As gradients in temperature and water vapour mixing ratio increase between the CAS and the PBL, the sensible and latent heat fluxes increase, respectively. The SiB model, in point simulations, has been shown to have a warm bias at WLEF, producing too much sensible heat flux and a high Bowen ratio (Baker et al., 2003) and this bias is also present in the SiB–RAMS coupled model (Denning et al., 2003). Baker et al. (2003) hypothesize that this bias is due to nearby wetlands not being simulated by the model.

The warming and drying of the atmosphere can close or open leaf stomata in an evolved response to limit water loss. Closing the stomata limits transpiration, thus shifting the Bowen ratio in favour of sensible heat flux. In addition, closing the stomata reduces carbon assimilation, increasing NEE and the CO_2 concentration. Cloud cover, radiation and regional geopotential gradients are tied to PBL temperature and moisture (Stull, 1988) so the large-scale weather is also modified. Reduced cloud cover over the eastern United States and Midwest, associated with a drier PBL, allows more solar radiation to reach the ground, increasing the surface energy budget and amending sensible and latent heat fluxes. In a few small regions where cloud cover was increased and less solar radiation was able to reach the ground, the surface heat budget was decreased. As the surface heat budget changes, so also does the simulated entrainment buoyancy

flux at the top of the PBL through the proportionality between them.

The sensible heat flux of the control case was similar to that observed in September and too great in July and August. The additional entrainment produced larger sensible heat fluxes and so was less representative of the observations. However, enhanced entrainment from overshooting thermals improved estimates of latent heat flux during all 3 months. The latent heat flux of the control case was too little and the additional entrainment increased this flux.

4.2. *NARR comparison*

Figure 5 compares the model results to the North American Regional Reanalysis (NARR; Mesinger et al., 2006) over the time–mean of the months of July, August and September. The left column shows the results of the control model minus the NARR while the right column shows the differences between the enhanced entrainment case and the reanalysis. When examining this figure, it is important to remember that the lateral boundaries of the SiB–RAMS model are nudged to the NCEP Eta model output and so should not be used for comparison.

The top row shows the model CAS temperature compared to the NARR 2 m temperature. This temperature is at the land–atmosphere interface and is impacted by the complex interactions of radiation, advection and sensible heat flux. It is important for determining the vegetative stress and therefore the NEE and CO_2 concentration. The CAS temperature is prognosed by SiB and is therefore valid only on land. The enhanced entrainment parameterization warmed the air within the PBL everywhere (Fig. 7b), but the effect on the CAS temperature was not quite as simple. Although the temperature increased in much of the domain, the states along the Gulf Coast actually

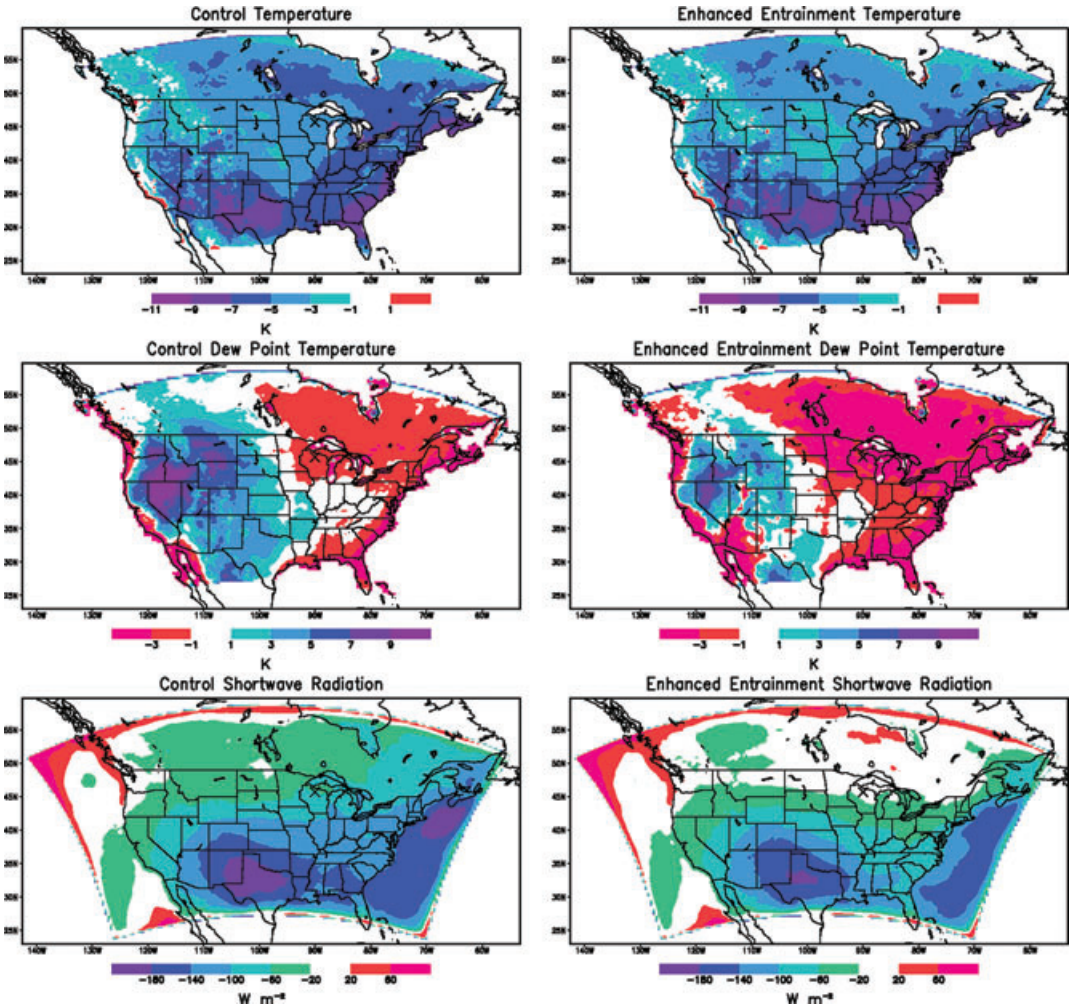

Fig. 5. Comparison between the North American Regional Reanalysis (NARR) product and the control (left) and enhanced entrainment ($\alpha = 0.2$; right) models for 2 m temperature (top), 2 m dew point temperature (middle) and downward shortwave radiation (bottom). The X in this and all subsequent figures marks the WLEF tower.

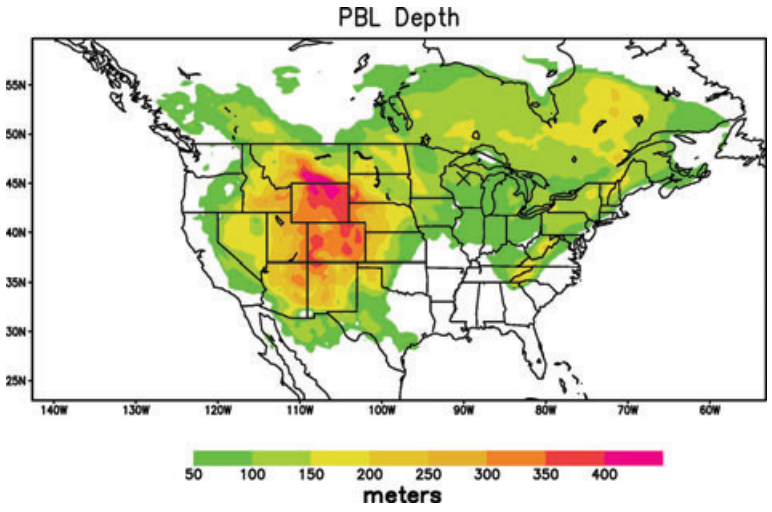

Fig. 6. Effect of entrainment from overshooting thermals (enhanced entrainment case minus control case) on PBL depth (m) in the time–mean from July through September including both daytime and nighttime values.

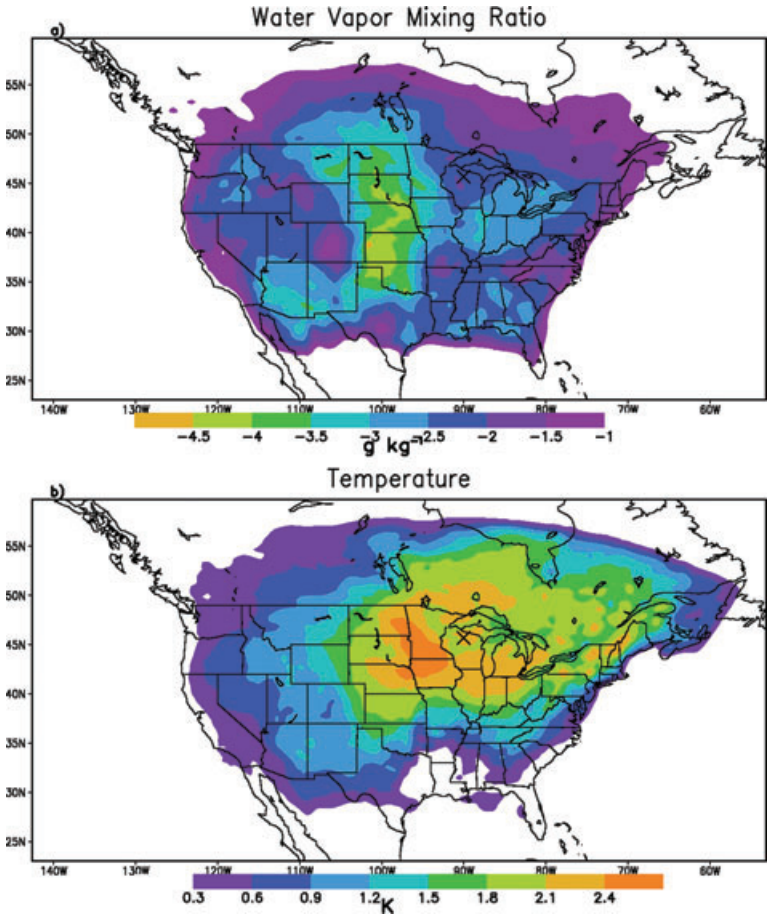

Fig. 7. Effect of entrainment from overshooting thermals (enhanced entrainment case minus control case) on (a) water vapour mixing ratio (g kg^{-1}) and (b) temperature (K) at 30 m in the time–mean from July through September.

experienced a cooling. When compared to the NARR, this indicated a weakness of the model. However, in the upper Midwest, including WLEF, the northeastern United States, and southeastern Canada, warmer temperatures indicated an improvement in the simulation results and a closer match to the reanalysis result.

The middle row compares the CAS dew point temperature, computed from SiB prognostic variables, to the NARR 2 m dew point temperature. The dew point temperature is a measure of the amount of water vapour surrounding the vegetation and is important for calculations of vegetative stress. It therefore impacts NEE and CO_2 concentration through its impact on stomatal

conductance. The CAS dries under enhanced entrainment, producing a decrease in the dew point temperature. In the Midwest, including the WLEF tower, the control simulation is too dry compared to the NARR and a further drying through enhanced entrainment worsens the problem. The result also degrades in southeastern Canada and in the southeastern United States. In the western states, however, where the control model is too moist, a drying improves the result. This illustrates the spatial variability of the response of the model to the parameterization.

Because more downward shortwave radiation reaches the surface on clear days than on days with heavy cloud cover, the shortwave radiation gives an indication to the amount of cloud cover. Over much of the domain, specifically the northeastern United States and southeastern Canada, the shortwave radiation is increased. This is important for photosynthesis because photosynthetic rates increase with increasing solar radiation up to a saturation amount. This affects the NEE (Fig. 10) and consequently the CO_2 concentration in addition to the sensible and latent heat fluxes. In general, both models predict less downward solar radiation than the NARR, indicating cloudier conditions, with the enhanced entrainment simulation showing an improvement over the control simulation in areas such as southern Canada and along the Gulf Coast. Although the decreased cloud cover would lead to increased PBL temperatures, idealized simulations by McGrath-Spangler et al. (2009) show that the qualitative results of this study are independent of changes in cloud cover.

Comparisons to the NARR data highlight the spatial inhomogeneity of the model response to the enhanced entrainment parameterization, the dependence upon the underlying surface conditions, and the complex interactions between the land surface and the atmosphere. The following subsection examines these points in further detail in direct comparisons between the two simulations.

4.3. Regional comparison

The following figures represent the time–mean differences between the enhanced entrainment and control cases averaged over the months of July, August and September. These difference plots show the impact of overshooting thermals on the model environment.

Figure 6 shows the impact of the enhanced entrainment parameterization on the simulated PBL. Enhanced entrainment produced, on average, a 70 m (11%) deeper PBL. The largest increases of around 300 to 400 m occurred over the dry

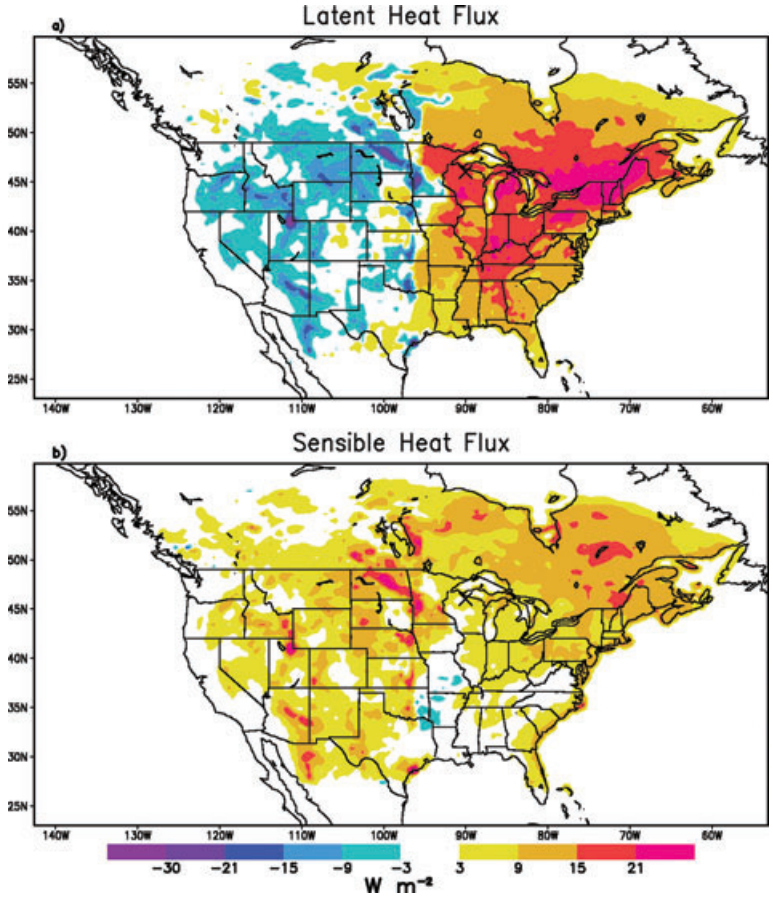

Fig. 8. Effect of entrainment from overshooting thermals (enhanced entrainment case minus control case) on (a) latent heat flux (W m^{-2}) and (b) sensible heat flux (W m^{-2}) in the time–mean from July through September.

Rocky Mountain region where the Bowen ratio was largest. Enhanced entrainment is proportional to the surface buoyancy flux ($H = \overline{\rho} c_p \overline{w'\theta_v'}$)

$$H \approx Q_H + \frac{0.61 c_p \theta Q_E}{L}, \tag{2}$$

where Q_H represents the sensible heat flux, Q_E the latent heat flux, c_p the specific heat at constant pressure and L the latent heat of vapourization. This equation is derived using Reynolds averaging and a few simplifying assumptions. Therefore, for a given amount of radiation, the larger the Bowen ratio (Q_H large compared to Q_E) the larger the heat flux and by extension the entrainment flux and the influence on the PBL depth.

Figure 7a shows a map of the difference in water vapour mixing ratio between the two cases. The domain-wide decrease in mixing ratio had an average of 18% (1.5 g kg^{-1}). The largest decrease was just downstream of the Rocky Mountains, where PBL depth was most affected, from North Dakota south into northern Texas. When the air left the Rocky Mountain region, it characterized the accumulated effect of the enhanced entrainment. Large decreases in mixing ratio were also present in the Midwest from Illinois into Ohio and Michigan and along the Mexican border with Arizona and New Mexico. Smaller decreases were present in central Colorado and the Carolinas.

Figure 7b shows the map of average change in temperature due to the enhanced entrainment. Temperature increased everywhere with an average increase of 4.3% (0.7 °C). The greatest increases occurred in the eastern sections of the Dakotas, Nebraska and Minnesota down into Iowa. Because the lateral boundaries were nudged to the same values in both cases, temperature changes were weakest there.

Figure 8a is a map of the time–mean difference in latent heat flux from the CAS to the boundary layer. On average, the latent heat flux was increased by just over 12% (12.7 W), mostly in the eastern half of the United States. The sharp transition between a decrease in latent heat flux in the west and an increase in the east is a result of a coupled surface–atmosphere response to the modifications to the PBL top entrainment. The surface response to the warmer and drier PBL is dependent upon several factors including vegetation type and prevailing surface conditions. In the west, increased solar radiation imposes an ecophysiological stress that the vegetation responds to by closing their stomates, limiting transpiration and decreasing the latent heat flux. The eastern United States is not as water limited as in the west and although overall stress is increased, the additional radiation benefit compensates for the drier conditions, allowing plant stomates to open further to permit more carbon assimilation. More water is lost through transpiration and the latent heat flux is increased.

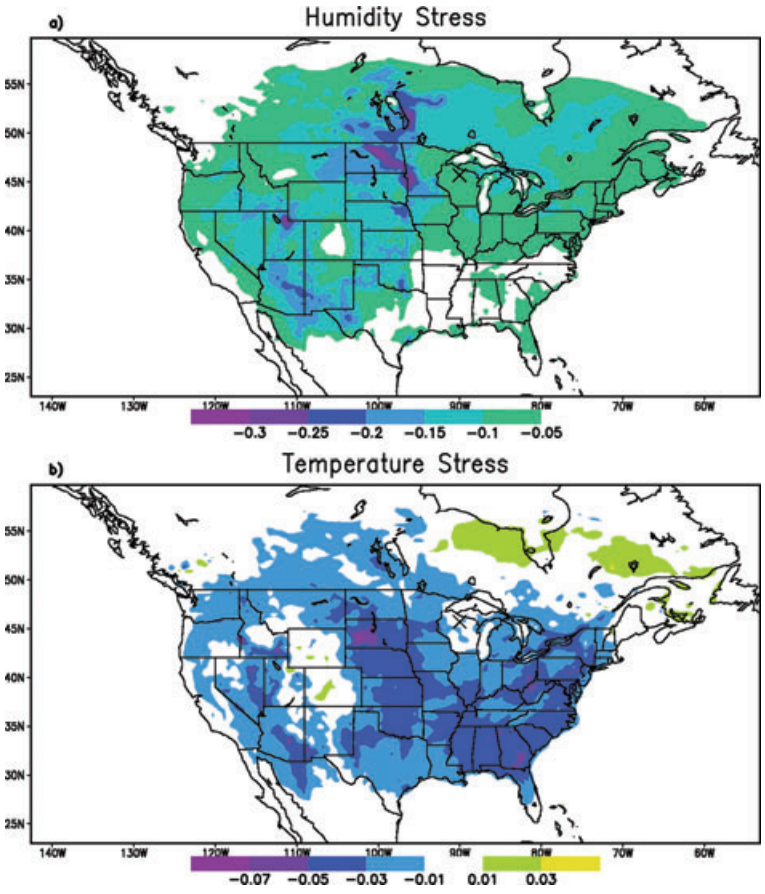

Fig. 9. Effect of entrainment from overshooting thermals (enhanced entrainment case minus control case) on (a) humidity stress and (b) temperature stress in the time–mean from July through September.

Figure 8b is a map of the differences in sensible heat flux between the CAS and the boundary layer for the enhanced entrainment and control cases. Sensible heat flux, on average, increased by almost 4 W in the time period of July through September. A drier, deeper PBL resulted in fewer clouds and more solar radiation reaching the ground. This allowed both the sensible and latent heat fluxes to increase. For this study, the addition of the enhanced entrainment parameterization produced a nearly 1% decrease in cloud cover over a large portion of the domain. This decrease extended southeastwards from Montana to Florida and the Gulf of Mexico, up along the United States eastern coast and then up into Canada and the northern boundary of the domain. Portions of southeastern Montana and Idaho as well as parts of the Gulf Coast and Atlantic experienced an increase in the amount of cloud cover, however, on the average, the parameterization produced a 0.3% decrease in the amount of cloud cover (not shown). This effect is only relevant when there are variations in cloud cover between the control and enhanced entrainment cases.

Figure 9a shows the physiological stress on vegetation due to low humidity. Stomata close to restrict water vapour loss when the leaf surface dries (Ball et al., 1987; Collatz et al., 1991; Bonan et al., 2002). This is expressed in the model as a decreased stress parameter. The stress parameters are dimensionless multiplicative factors that modify the stomatal conductance. They are scaled between 1 for optimal conditions (resulting in unstressed conductance and fully open stomates) to 0 (severely stressed conductance) when environmental conditions decrease the stomatal opening (Sellers et al., 1997). Stomatal closing results in decreased transpiration, reduced latent heat flux, and increased sensible heat flux. This acts to reduce the boundary layer humidity and increase its temperature. Because a smaller stomatal opening produces decreased carbon assimilation, this parameter also indicates CO_2 concentration changes. The drying associated with entrainment from overshooting thermals produced a 10% change in the humidity stress parameter, indicating diminished stomatal conductance.

The effect of entraining thermals on physiological stress due to departures from a moderate temperature is illustrated in Fig. 9b. This parameter has the same effect on stomatal conductance as the humidity parameter. Although warmer temperatures were present everywhere as was shown in Fig. 7b, the temperature stress is not as straightforward. In regions where the summer temperature was already on the warm end of optimal vegetative temperatures, warmer temperatures due to enhanced entrainment produced smaller stomatal conductance. However, in relatively cool locations, such as northern latitudes and at high altitude, warmer temperatures were more moderate for the plants and stomatal conductance increased. In regions of Canada and along the Rocky Mountains, warmer temperatures were actually beneficial to the plants.

Stomatal conductance controls the amount of carbon that the vegetation is able to assimilate and therefore the NEE (Fig. 10).

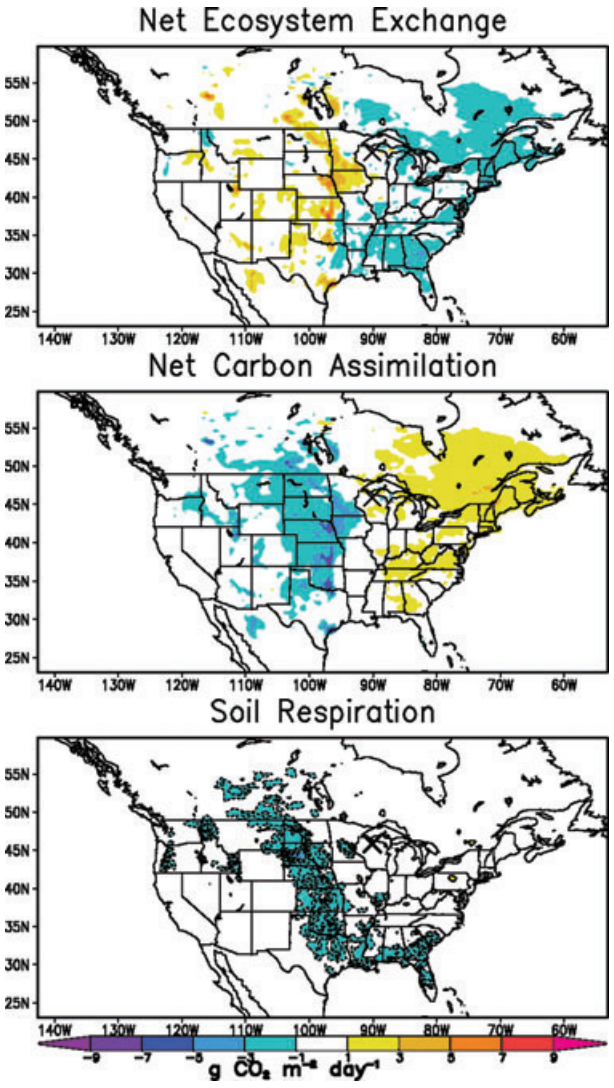

Fig. 10. Effect of entrainment from overshooting thermals (enhanced entrainment case minus control case) on (a) net ecosystem exchange (g CO_2 m^{-2} day^{-1}), (b) carbon assimilation (g CO_2 m^{-2} day^{-1}) and (c) soil respiration (g CO_2 m^{-2} day^{-1}) in the time–mean from July through September.

NEE (Fig. 10a) is decreased from the Mississippi River eastwards to the Atlantic Ocean while, in the western United States, NEE is increased. Most of these changes are due to changes in carbon assimilation (Fig. 10b). Assimilation was increased in the eastern half of the domain, mostly due to decreased cloud cover. Fewer clouds permit more solar radiation to penetrate to the surface, allowing more photosynthesis by the surface vegetation. The strongest increase in solar radiation (about 20 W m^{-2} in the average) occurred primarily in the eastern United States and southeastern Canada (not shown). Decreased carbon assimilation along the Great Plains was a result of warmer and drier conditions producing a closing of plant stomata. Re-

duced soil respiration (Fig. 10c) through the Great Plains and along the Gulf of Mexico was a result of slightly reduced soil moisture. Enhanced soil respiration in the Ohio valley and New England was a result of warmer soil temperatures.

Figure 11 illustrates the CO_2 concentration effects at 500 m caused by the parameterized PBL top entrainment. Lower concentrations are present in southeastern Canada and New England because lower temperature stress (Fig. 9b) and greater solar radiation allowed greater carbon assimilation (Fig. 10b) through increased stomatal conductance in this region. Higher CO_2 concentrations centred on the upper Midwest are a result of reduced assimilation (Fig. 10b) from the increased stress due to warmer and drier conditions (Fig. 9) and a deeper PBL (Fig. 6). The dilution of the carbon assimilation impact by the deeper PBL in addition to the weaker uptake of CO_2 produced higher CO_2 concentrations. The combination of a weak PBL depth response (Fig. 6), greater carbon assimilation (Fig. 10b) from increased solar radiation and weaker soil respiration (Fig. 10c) due to decreased soil moisture led to lower CO_2 concentrations over the states along the Gulf of Mexico, including Louisiana, Alabama and Florida. On average, there was no change in CO_2 concentration, but the gradients of CO_2 were largely impacted by entrainment. Enhanced entrainment produces a 7 ppmv gradient in CO_2 at 500 m above ground level from the eastern Minnesota/Iowa border to the border of New York and Canada, relative to the control case. These simulated differences in spatial patterns of atmospheric CO_2 suggest that the degree of entrainment at the PBL top could be an important influence on source/sink estimation by transport inversion.

An entrainment parameterization was added to SiB–RAMS to include the effects of overshooting thermals. The parameterization warms and dries the boundary layer while cooling and moistening the inversion layer through a downward buoyancy flux at the PBL top. The enhancement of entrainment effects increased the model estimate of the PBL depth in a simulation representing the weather conditions of late summer 1999.

The monthly mean diurnal cycle of PBL depth in July, August and September at the WLEF tower in northern Wisconsin was simulated better when the enhanced entrainment was included. This depth is important for CO_2 studies as an error in PBL depth relates linearly to errors in CO_2 concentration. It was seen in Fig. 11 that this could impact horizontal gradients of CO_2 and produce a model–observation mismatch even when the simulated fluxes are correct. Because most CO_2 concentration measurements are made near the surface and depend on the depth of the PBL and source/sink estimates of carbon from inversion studies depend on the CO_2 concentrations, correcting the PBL depth should also improve the source/sink estimates.

Overshooting thermals produce a complex interaction of PBL processes. In addition to increasing the PBL depth and modifying CO_2 concentration gradients, overshooting thermals and their associated entrainment impact temperature and water vapour mixing ratios which, in turn, impact sensible and latent heat fluxes and vegetative response. The warmer and drier conditions at the leaf surface alter stomatal conductance, modifying the Bowen ratio and cloud cover. Closing of the stomata produces decreased carbon assimilation which, when combined with the dilution effect of a deeper PBL, produces higher CO_2 concentrations. Decreased cloud cover results in greater net radiation at the surface and a greater surface heat flux. Given that the buoyancy flux at the top of the PBL is proportional to that at the surface, this produces a positive feedback and a large impact on the PBL and the land surface. Overshooting thermals, although small, can interact to produce large-scale changes in the land–atmosphere interaction.

5. Acknowledgments

We thank Ken Davis at The Pennsylvania State University and Oak Ridge National Laboratory for providing public access to data used in this study. The NARR data for this study are from the Research Data Archive (RDA), which is maintained by the

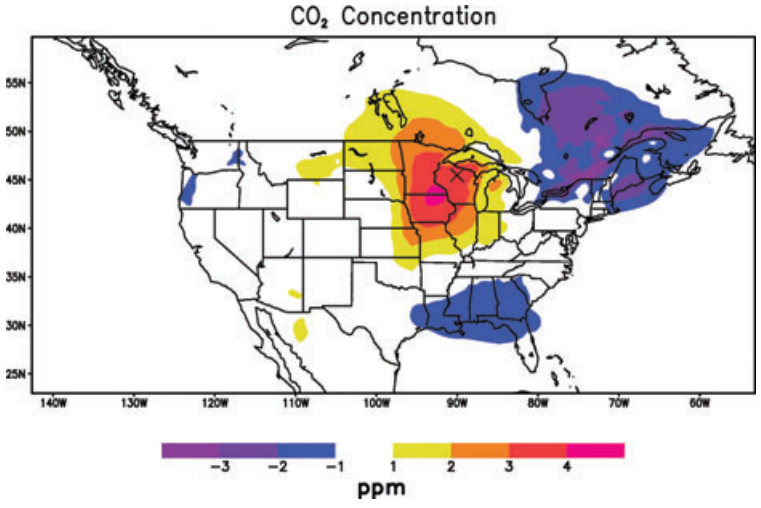

Fig. 11. Effect of entrainment from overshooting thermals (enhanced entrainment case minus control case) on CO_2 concentration (ppm) at 500 m in the time–mean from July through September.

Computational and Information Systems Laboratory (CISL) at the National Center for Atmospheric Research (NCAR). NCAR is sponsored by the National Science Foundation (NSF). The original data are available from the RDA (http://dss.ucar.edu) in data set number ds608.0. We are grateful to Ian Baker for many thoughtful discussions and to Mark Branson for his help with the NARR data. We would also like to thank two anonymous reviewers who have improved the quality of this paper substantially. This research was supported by National Aeronautics and Space Administration grant NNG05GD15G.

References

Andres, R. J., Marland, G., Fung, I. and Matthews, E. 1996. A $1^\circ \times 1^\circ$ distribution of carbon dioxide emissions from fossil fuel consumption and cement manufacture, 1950–1990. *Global Biogeochem. Cy.* **10**, 419–429.

Angevine, W. M., Avery, S. K., Ecklund, W. L. and Carter, D. A. 1993. Fluxes of heat and momentum measured with a boundary-layer wind profiler radar-radio acoustic sounding system. *J. Appl. Meteorol.* **32**, 73–80.

Angevine, W. M., Doviak R. J. and Sorbjan, Z. 1994a. Remote sensing of vertical velocity variance and surface heat flux in a convective boundary layer. *J. Appl. Meteorol.* **33**, 977–983.

Angevine, W. M., White, A. B. and Avery, S. K. 1994b. Boundary-layer depth and entrainment zone characterization with a boundary-layer profiler. *Bound. -Layer Meteorol.* **68**, 375–385.

Angevine, W. M., Bakwin, P. S. and Davis, K. J. 1998. Wind profiler and RASS measurements compared with measurements from a 450-m-tall tower. *J. Atmos. Oceanic Technol.* **15**, 818–825.

Avissar, R. 1991. A statistical-dynamical approach to parameterize subgrid-scale land-surface heterogeneity in climate models. *Surv. Geophys.* **12**, 155–178.

Avissar, R. and Pielke, R. A. 1989. A parameterization of heterogeneous land surfaces for atmospheric numerical models and its impacts on regional meteorology. *Mon. Weather Rev.* **117**, 2113–2136.

Ayotte, K. W., Sullivan, P. P., Andrén, A., Doney, S. C., Holtslag, A. A. M. and co-authors. 1996. An evaluation of neutral and convective planetary boundary layer parameterizations relative to large eddy simulation. *Bound. -Layer Meteorol.* **79**, 131–175.

Baker, D. F., Law, R. M., Gurney, K. R., Rayner, P., Denning, A. S. and co-authors. 2006. TransCom 3 inversion intercomparison: impact of transport model errors on the interannual variability of regional CO_2 fluxes, 1988–2003. *Global Biogeochem. Cyc.* **20**, GB1002, doi:10.1029/2004GB002439.

Baker, I., Denning, A. S., Hanan, N., Prihodko, L., Uliasz, M. and co-authors. 2003. Simulated and observed fluxes of sensible and latent heat and CO_2 at the WLEF-TV tower using SiB2.5. *Glob. Change Biol.* **9**, 1262–1277.

Bakwin, P. S., Tans, P. P., Hurst, D. F. and Zhao, C. 1998. Measurements of carbon dioxide on very tall towers: results of the NOAA/CMDL program. *Tellus* **50B**, 401–415.

Ball, J. T., Woodrow, I. E. and Berry, J. A. 1987. A model predicting stomatal conductance and its contribution to the control of photosynthesis under different environmental conditions. In: *Progress in Photosynthesis Research* (ed. J. Biggens). Martinus-Nijhoff Publishers, Dordrecht, the Netherlands 221–224.

Beljaars, A. C. M and Betts, A. K. 1992. Validation of the boundary layer representation in the ECMWF model. In: *ECMWF Seminar Proceedings, 7–11 September 1992, Validation over Europe, Vol II,* Reading, 159–195.

Berger, B. W., Davis, K. J., Yi, C., Bakwin, P. S. and Zhao C. L. 2001. Long-term carbon dioxide fluxes from a very tall tower in a northern forest: flux measurement methodology. *J. Atmos. Ocean. Tech.* **18**, 529–542.

Betts, A. K. 1973. Non-precipitating cumulus convection and its parameterization. *Q. J. Roy. Meteor. Soc.* **99**, 178–196.

Bonan, G. B., Lewis, S., Kergoat, L. and Oleson, K. W. 2002. Landscapes as patches of plant functional types: an integrating concept for climate and ecosystem models. *Global Biogeochem. Cy.* **16**, 5.1–5.23.

Carson, D. J. 1973. The development of a dry inversion-capped convectively unstable boundary layer. *Q. J. Roy. Meteor. Soc.* **100**, 450–467.

Collatz, G. J., Ball, J. T., Grivet, C. and Berry, J. A. 1991. Physiological and environmental regulation of stomatal conductance, photosynthesis and transpiration: a model that includes a laminar boundary layer. *Agric. Forest Meteorol.* **54**, 107–136.

Corbin, K. D., Denning, A. S., Lu, L., Wang, J.-W. and Baker, I. T. 2008. Possible representation errors in inversions of satellite CO_2 retrieval. *J. Geophys. Res.* **113**, D02301, doi:10.1029/2007JD008716.

Davis, K. J., Lenschow, D. H., Oncley, S. P., Kiemle, C., Ehret, G. and co-authors. 1997. Role of entrainment in surface-atmosphere interactions over the boreal forest. *J. Geophys. Res.* **102**, D24, 29219–29230, doi:10.1029/97JD02236.

Davis, K. J., Bakwin, P. S., Yi, C., Berger, B. W., Zhao, C. and co-authors. 2003. The annual cycles of CO_2 and H_2O exchange over a northern mixed forest as observed from a very tall tower. *Glob. Change Biol.* **9**, 1278–1293.

Deardorff, J. W. 1974. Three-dimensional numerical study of the height and mean structure of a heated planetary boundary layer. *Bound -Layer Meteorol.* **7**, 81–106.

Denning, A. S., Fung, I. Y. and Randall, D. A. 1995. Latitudinal gradient of atmospheric CO_2 due to seasonal exchange with land biota. *Nature* **376**, 240–243.

Denning, A. S., Collatz, J. G., Zhang, C., Randall, D. A., Berry, J. A. and co-authors. 1996a. Simulations of terrestrial carbon metabolism and atmospheric CO_2 in a general circulation model. Part 1: Surface carbon fluxes. *Tellus* **48B**, 521–542.

Denning, A. S., Randall, D. A., Collatz, G. J. and Sellers, P. J. 1996b. Simulations of terrestrial carbon metabolism and atmospheric CO_2 in a general circulation model. Part 2: Spatial and temporal variations of atmospheric CO_2. *Tellus* **48B**, 543–567.

Denning, A. S., Takahashi, T. and Friedlingstein P. 1999. Can a strong atmospheric CO_2 rectifier effect be reconciled with a "reasonable carbon budget? *Tellus* **51B**, 249–253.

Denning, A. S., Nicholls, M., Prihodko, L., Baker, I., Vidale, P.-L. and co-authors. 2003. Simulated variations in atmospheric CO_2 over a Wisconsin forest using a coupled ecosystem-atmosphere model. *Glob. Change Biol.* **9**, 1241–1250.

Denning, A. S., Zhang, N., Yi, C., Branson, M., Davis, K. and co-authors. 2008. Evaluation of modeled atmospheric boundary layer depth at the WLEF tower. *Agric. Forest Meteorol.* **148**, 206–215.

Ecklund, W. L., Carter, D. A. and Balsley, B. B. 1988. A UHF wind profiler for the boundary layer: brief description and initial results. *J. Atmos. Ocean. Tech.* **5**, 432–441.

Freitas, S. R., Longo, K., Silva Dias, M., Silva Dias, P., Chatfield, R. and co-authors. 2006. The coupled aerosol and tracer transport model to the Brazilian developments on the Regional Atmospheric Modeling System: validation using direct and remote sensing observations. *International Conference on Southern Hemisphere Meteorology and Oceanography (ICSHMO)*, Volume**8**, 101–107. CD-ROM. ISBN 85–17-00023-4.

Gerbig, C., Lin, J. C., Wofsy, S. C., Daube, B. C., Andrews, A. E. and co-authors. 2003. Toward constraining regional-scale fluxes of CO_2 with atmospheric observations over a continent: 1. Observed spatial variability from airborne platforms. *J. Geophys. Res.* **108**, D24, doi:10.1029/2002JD003018.

Gurney, K. R., Law, R. M., Denning, A. S., Rayner, P. J., Baker, D. and co-authors. 2002. Towards robust regional estimates of CO_2 sources and sinks using atmospheric transport models. *Nature* **415**, 626–630.

Gurney, K. R., Law, R. M., Denning, A. S., Rayner, P. J., Baker, D. and co-authors. 2003. TransCom 3 CO_2 inversion intercomparison: 1. Annual mean control results and sensitivity to transport and prior flux information. *Tellus* **55B**, 555–579.

Hansen, M., DeFries, R., Townshend, J. R. G. and Sohlberg, R. 2000. Global land cover classification at 1km resolution using a decision tree classifier. *Int. J. Remote Sens.* **21**, 1331–1365.

Kawa, S. R., Erickson III, D. J., Pawson, S. and Zhu, Z. 2004. Global CO_2 transport simulations using meteorological data from the NASA data assimilation system. *J. Geophys. Res.* **109**, D18312, doi:10.1029/2004JD004554.

Liu, Y., Weaver, C. P. and Avissar, R. 1999. Toward a parameterization of mesoscale fluxes and moist convection induced by landscape heterogeneity. *J. Geophys. Res.* **104**(D16), 19515–19533.

Marland, G., Boden, T. A. and Andres, R. J. 2005. Global, regional and national CO_2 emissions, In: *Trends: A compendium of Data on Global Change*. Carbon Dioxide Information Analysis Center, Oak Ridge National Laboratory, U.S. Department of Energy, Oak Ridge, TN. Available from http://cdiac.ornl.gov/trends/emis/em_cont.htm. Accessed 3 April 2008.

McGrath-Spangler, E. L., Denning, A. S., Corbin, K. D. and Baker, I. T. 2009. Sensitivity of land-atmosphere exchanges to overshooting PBL thermals in an idealized coupled model. *J. Adv. Model. Earth Syst.* **1**(14), doi:10.3894/JAMES.2009.1.14.

Mesinger, F., DiMego, G., Kalnay, E., Mitchell, K., Shafran, P. C. and co-authors. 2006. North American regional reanalysis. *B. Am. Meteorol. Soc.* **87**(3), 343–360.

Nicholls, M. E., Denning, A. S., Prihodko, L., Vidale, P. –L., Baker, I. and co-authors. 2004. A multiple-scale simulation of variations in atmospheric carbon dioxide using a coupled-biosphere-atmospheric model. *J. Geophys. Res.* **109**, D18117, doi:10.1029/2003JD004482.

Parazoo, N. C., Denning, A. S., Kawa, S. R., Corbin, K. D., Lokupitiya, R. S. and co-authors. 2008. Mechanisms for synoptic variations of atmospheric CO_2 in North America, South America, and Europe. *Atmos. Chem. Phys.* **8**, 7239–7254.

Pielke, R. A. and Avissar, R. 1990. Influence of landscape structure on local and regional climate. *Landscape Ecol.* **4**, 133–155.

Rayment, R. and Readings, C. J. 1974. A case study of the structure and energetics of an inversion. *Q. J. Roy. Meteor. Soc.* **100**, 221–233.

Sellers, P. J., Mintz, Y., Sud, Y. C. and Dalcher, A. 1986. A simple biosphere model (SiB) for use within general circulation models. *J. Atmos. Sci.* **43**, 505–531.

Sellers, P. J., Los, S. O., Tucker, C. J., Justice, C. O., Dazlich, D. A. and co-authors. 1996b. A revised land surface parameterization (SiB2) for atmospheric GCMs. Part II: The generation of global fields of terrestrial biophysical parameters from satellite data. *J. Climate* **9**, 706–737.

Sellers, P. J., Randall, D. A., Collatz, G. J., Berry, J. A., Field, C. B. and co-authors. 1996a. A revised land surface parameterization (SiB2) for atmospheric GCMs, Part 1: Model formulation. *J. Climate* **9**, 676–705.

Sellers, P. J., Dickinson, R. E., Randall, D. A., Betts, A. K., Hall, F. G. and co-authors. 1997. Modeling the exchanges of energy, water, and carbon between continents and the atmosphere. *Science* **275**, 502–509.

Stull, R. B. 1976. The energetics of entrainment across a density interface. *J. Atmos. Sci.* **33**, 1260–1267.

Stull, R. B. 1988. *An Introduction to Boundary Layer Meteorology*. Kluwer Academic Publishers, Norwell, MA, 666pp.

Sullivan, P. P., Moeng, C.-H., Stevens, B., Lenschow, D. H. and Mayer, S. D. 1998. Structure of the entrainment zone capping the convective atmospheric boundary layer. *J. Atmos. Sci.* **55**, 3042–3064.

Takahashi, T., Sutherland, S. C., Sweeney, C., Poisson, A., Metzl, N. and co-authors. 2002. Global sea-air CO_2 flux based on climatological surface ocean pCO_2, and seasonal, biological, and temperature effects. *Deep-Sea Res. Part II* **49**, 1601–1622.

Wang, J.-W., Denning, A. S., Lu, L., Baker, I. T., Corbin, K. D. and co-authors. 2007. Observations and simulations of synoptic, regional, and local variations in atmospheric CO_2. *J. Geophys. Res.* **112**, D04108, doi:10.1029/2006JD007410.

Weaver, C. P. and Avissar, R. 2001. Atmospheric disturbance caused by human modification of the landscape. *B. Am. Meteorol. Soc.* **82**(2), 269–281.

White, A. B., Fairall, C. W. and Thompson, D. W. 1991. Radar observations of humidity variability in and above the marine atmospheric boundary layer. *J. Atmos. Ocean. Tech.* **8**, 639–658.

Willis, G. E. and Deardorff, J. W. 1974. A laboratory model of the unstable planetary boundary layer. *J. Atmos. Sci.* **31**, 1297–1307.

Yi, C., Davis, K. J., Berger, B. W. and Bakwin, P. S. 2001. Long-term observations of the dynamics of the continental planetary boundary layer. *J. Atmos. Sci.* **58**, 1288–1299.

Yi, C., Davis, K. J., Bakwin, P. S., Denning, A. S., Zhang, N. and co-authors. 2004. Observed covariance between ecosystem carbon exchange and atmospheric boundary layer dynamics at a site in northern Wisconsin. *J. Geophys. Res.* **109**, D08302, doi:10.1029/2003JD004164.

Zhang, N. 2002. Observations and simulations of the planetary boundary layer at a tall tower in northern Wisconsin. M.S. thesis. Colorado State University, Fort Collins, 71.

Zupanski, D., Denning, A. S., Uliasz, M., Zupanski, M., Schuh, A. E. and co-authors. 2007. Carbon flux bias estimation employing Maximum Likelihood Ensemble Filter (MLEF). *J. Geophys. Res.* **112**, D17107, doi:10.1029/2006JD008371.